The effect of interpolating low amplitude leads on the inverse reconstruction of cardiac electrical activity

Computers in Biology and Medicine 136 (2021) 104666

Contents lists available at ScienceDirect

Computers in Biology and Medicine

journal homepage: www.elsevier.com/locate/compbiomed

The effect of interpolating low amplitude leads on the inverse reconstruction of cardiac electrical activity

Ali S. Rababah [a,*], Laura R. Bear [b], Yesim Serinagaoglu Dogrusoz [c], Wilson Good [d], Jake Bergquist [d], Job Stoks [e], Rob MacLeod [d], Khaled Rjoob [a], Michael Jennings [a], James Mclaughlin [a], Dewar D. Finlay [a]

[a] School of Engineering, Ulster University, Northern Ireland, UK
[b] IHU LIRYC, Université de Bordeaux, CRCTB Inserm U1045, Bordeaux, France
[c] Electrical-Electronics Engineering Department, Middle East Technical University, Ankara, Turkey
[d] Scientific Computing and Imaging Institute, University of Utah, SLC, UT, USA
[e] Department of Cardiology, Maastricht University, Maastricht, the Netherlands

ARTICLE INFO

Keywords:
Inverse-forward interpolation
Hybrid interpolation
Laplacian interpolation
Low amplitude leads
Inverse reconstruction of cardiac electrical activity
Potential maps
Activation times maps

ABSTRACT

Electrocardiographic imaging is an imaging modality that has been introduced recently to help in visualizing the electrical activity of the heart and consequently guide the ablation therapy for ventricular arrhythmias. One of the main challenges of this modality is that the electrocardiographic signals recorded at the torso surface are contaminated with noise from different sources. Low amplitude leads are more affected by noise due to their low peak-to-peak amplitude. In this paper, we have studied 6 datasets from two torso tank experiments (Bordeaux and Utah experiments) to investigate the impact of removing or interpolating these low amplitude leads on the inverse reconstruction of cardiac electrical activity. Body surface potential maps used were calculated by using the full set of recorded leads, removing 1, 6, 11, 16, or 21 low amplitude leads, or interpolating 1, 6, 11, 16, or 21 low amplitude leads using one of the three interpolation methods – Laplacian interpolation, hybrid interpolation, or the inverse-forward interpolation. The epicardial potential maps and activation time maps were computed from these body surface potential maps and compared with those recorded directly from the heart surface in the torso tank experiments. There was no significant change in the potential maps and activation time maps after the removal of up to 11 low amplitude leads. Laplacian interpolation and hybrid interpolation improved the inverse reconstruction in some datasets and worsened it in the rest. The inverse forward interpolation of low amplitude leads improved it in two out of 6 datasets and at least remained the same in the other datasets. It was noticed that after doing the inverse-forward interpolation, the selected lambda value was closer to the optimum lambda value that gives the inverse solution best correlated with the recorded one.

1. Introduction

Body surface potential mapping (BSPM) provides a remote measure of the electrical activity of the heart that can provide valuable information about cardiac electrophysiology. A larger number of electrodes than that used for the 12-lead ECG are typically required with anything between 32 and 250 used in practical systems. Combined with patient-specific heart-torso geometry obtained using MRI or CT scans, the inverse problem is solved to provide details of electrical activity on the heart's surface. This procedure is often referred to as electrocardiographic imaging (ECGI) which is effectively a non-invasive cardiac electroanatomic mapping modality that can reveal a range of detailed data that include epicardial electrograms, activation maps, and recovery sequences. Among other things, these data can help guide catheter ablation therapy of ventricular arrhythmias [1,2].

The mathematically computed cardiac electrical activity is sensitive to inaccuracies in both heart-torso geometry and body surface potential maps (BSPM) [3]. In the practical setting, it is not uncommon for the body surface information to be disrupted due to factors that include noise, accidental disconnection of electrodes, or intentional altering of electrode positions to facilitate other devices such as defibrillation pads or Carto patches. The impact of noise and different ECG signal

* Corresponding author. 302 Bradbury Court, Belfast, BT9 7JL, UK.
E-mail address: Rababah-a@ulster.ac.uk (A.S. Rababah).

https://doi.org/10.1016/j.compbiomed.2021.104666
Received 27 February 2021; Received in revised form 17 July 2021; Accepted 17 July 2021
Available online 21 July 2021

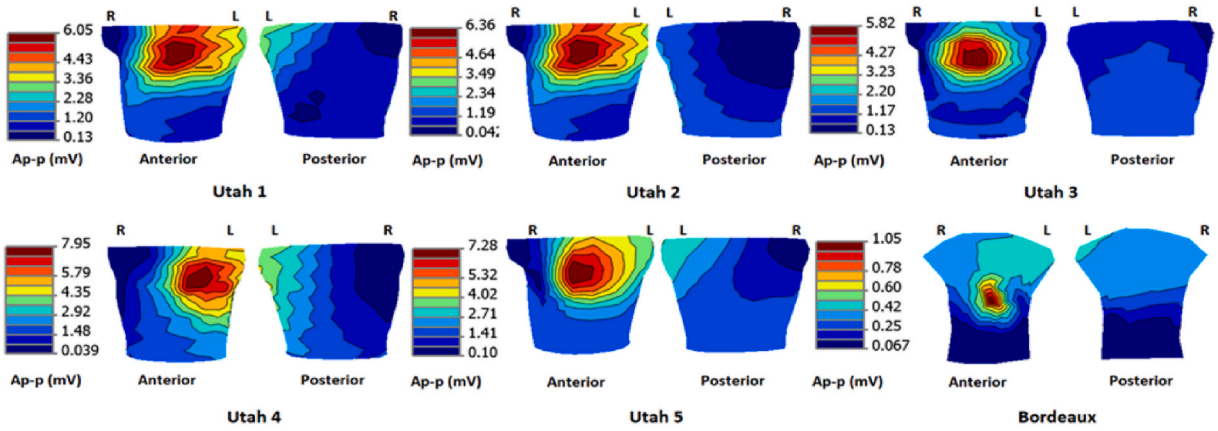

Fig. 1. Body surface maps that show the distribution of peak-to-peak amplitude ($A_{p\text{-}p}$) measured from 192 or 128 surface electrodes. The lowest amplitude leads are located at the right shoulder in Utah datasets and at the lower part of the torso in the Bordeaux dataset.

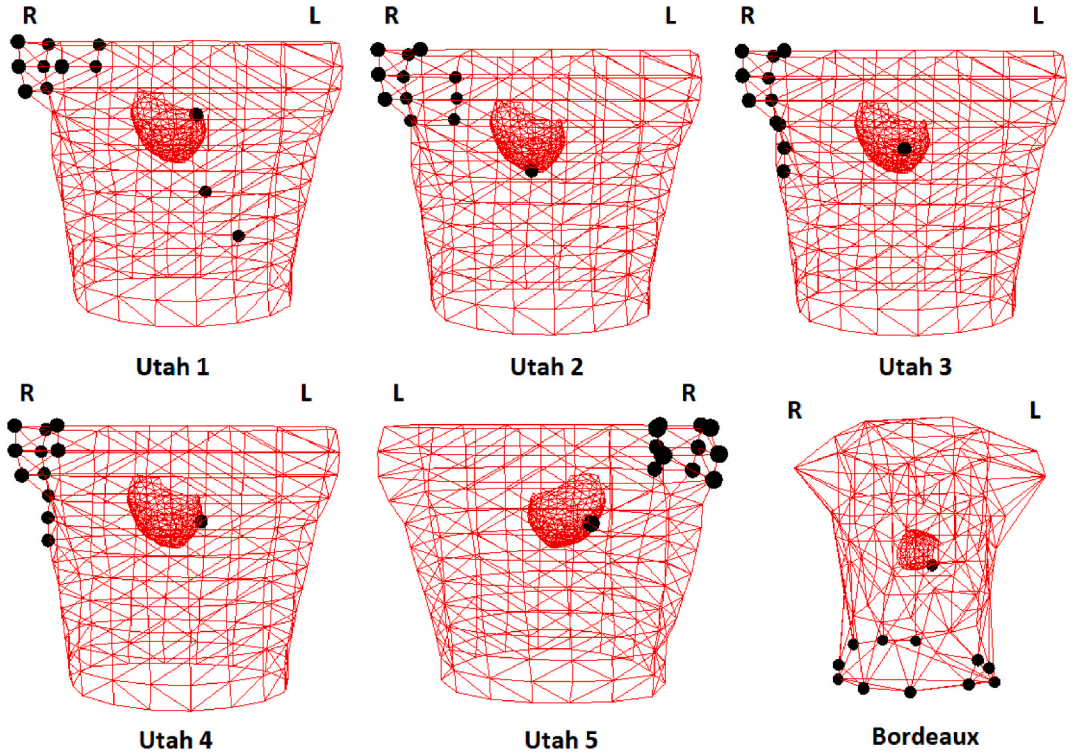

Fig. 2. The position of the removed/interpolated leads on the torso and their relative position to the stimulating electrode on the heart.

processing methods have been investigated by the signal processing group within the consortium for ECG imaging [4,5]. Several studies have also investigated the effect of missing body surface ECG information on the reconstructed cardiac signals and the effectiveness of different interpolation methods in alleviating this effect [6,7]. Furthermore, the effect of removing noise-contaminated leads on the accuracy of the inverse solution and consequently on the localization of the focus of premature ventricular complexes (PVCs) has been studied previously [8].

In a previous study, we demonstrated using a single dataset that removing the lowest amplitude signals (<0.2 mV peak to peak over the QRS complex) and replacing them with Laplacian interpolated signals improves the inverse reconstruction of cardiac electrical activity [9]. As the peak-to-peak amplitude depends on the distance from the potential source (the heart), and the location of the recording electrode with respect to the QRS axis, some locations on the torso are more prone to the effects of noise than others [9]. In the current paper, we aim to study this idea in more detail, by evaluating the impact on the inverse solution of removing or replacing low amplitude signals with interpolated signals. This work further builds on the previous study by incorporating additional datasets generated from a torso tank experiment where the heart was paced from 5 different locations. We also evaluate two alternative methods of interpolation, the inverse-forward method (IF) [10] and a hybrid interpolation scheme [11]. These interpolation methods have been previously investigated when the simulated region of missing data was over the heart [10,11]. However, this study focuses on interpolating low amplitude leads and its impact on the inverse solution.

Laplacian interpolation of body surface potential maps was firstly introduced by Oostendorp et al. [12]. It is based on computing the unknown potentials from the known potentials by minimizing the Laplacian of potential function at all points of the body surface [12]. This

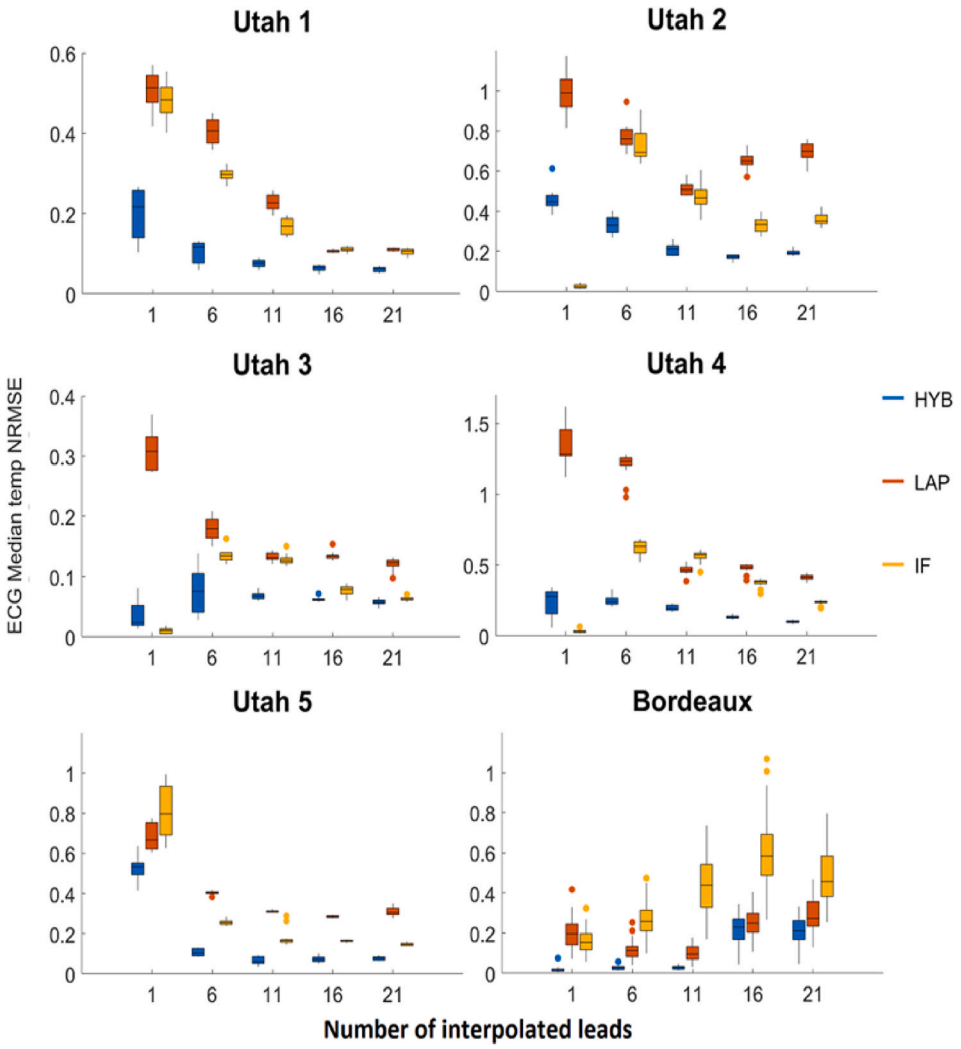

Fig. 3. The median of $NRMSE_{ECG}$ of ECGs (mV) for each of the six datasets. Each subplot shows the median of $NRMSE_{ECG}$ measured for HYB, LAP, and IF methods as the number of interpolated leads were increased. The median of $NRMSE_{ECG}$ values are expressed as median [lower quartile, upper quartile].

method has been used previously to standardize body surface potential data from different research centres [13,14]. It has also been investigated to study the impact of interpolating missing potentials on the inverse problem of electrocardiography [10,15]. The hybrid interpolation method combines Laplacian interpolation and principal component analysis (PCA) interpolation [11]. Principal component analysis (PCA) was previously used for temporal and spatial compression of BSPM [16,17]. In this study, the PCA method will be used as a part of the hybrid interpolation scheme [11,18]. The inverse forward interpolation was developed by Burnes et al. [10]. The potentials at an inner surface chosen between the torso and the heart were inversely computed from the measured torso potentials using the method of fundamental solutions. The interpolated potentials are then computed by forward transforming the inner surface potentials to the outer surface [10].

2. Methods

2.1. Bordeaux dataset

All experimental data were obtained in accordance with the guidelines from Directive 2010/63/EU of the European Parliament on the protection of animals used for scientific purposes and approved by the local ethical committee. The procedure is described in detail in Ref. [19]. Briefly, an explanted Langendorff-perfused pig's heart was suspended in an instrumented, human-shaped, electrolytic torso tank. Electrical potentials were recorded simultaneously from 128 tank electrodes (inter-electrode spacing 66 ± 24 mm) and 108 sock electrodes (inter-electrode spacing 9.9 ± 2.2 mm) at 2 kHz (BioSemi, the Netherlands). For this study, we used the data recorded with the heart paced from the right ventricular (RV) apex. Following that, 3D rotational fluoroscopy (Artis, Siemens) was used to acquire heart and tank geometries along with the locations of the recording electrodes.

2.2. Utah dataset

The experiment was performed under deep anesthesia using procedures approved by the Institutional Animal Care and Use Committee of the University of Utah and conformed to the Guide for the Care and Use of Laboratory Animals. The experimental setup and protocol were described in detail in Ref. [20]. Briefly, A canine heart was excised and mounted on a Langendorff's perfusion. It was perfused using a mixture of whole blood and Tyrode's solution. Arterial blood was supplied from a second canine under deep anesthesia. The venous blood was extracted from the right ventricle of the isolated heart and pumped into the jugular vein of the support dog. A tank shaped like a human torso was filled with an electrolytic solution (500 Ω cm) and the isolated, perfused canine heart was suspended in it. The dataset consists of signals recorded simultaneously from 192 torso-tank electrodes (with inter-electrode

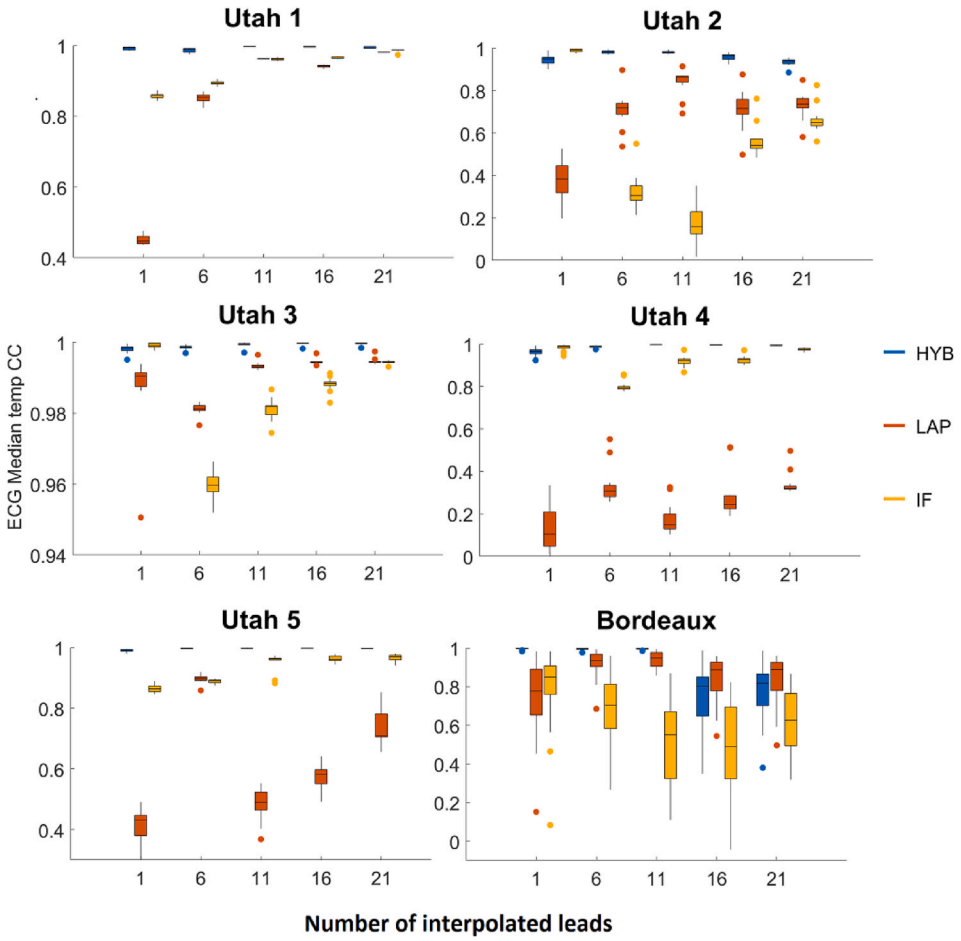

Fig. 4. The median of CC_{ECG} (mV) for each of the six datasets. Each subplot shows the median of CC_{ECG} measured for HYB, LAP, and IF methods as the number of interpolated leads were increased. The median of CC_{ECG} values are expressed as median [lower quartile, upper quartile].

spacing 40.2 ± 16.8 mm) and 247 epicardial sock electrodes (inter--electrode spacing 6.5 ± 1.3 mm). For this study, we used the data recorded when the heart was paced from 5 different epicardial locations: left ventricular (LV)-base, LV-apex, LV-septum, LV-free wall, and right ventricular (RV)-free wall from a series of intramural plunge needles using a 247-electrode epicardial sock. The epicardial, and torso tank electrodes were referenced to Wilson's central terminal and were sampled at 1 kHz simultaneously for 5 s during pacing. An MRI was used to generate the heart geometry and the tank was created via the digitization of the electrode position and manual triangulation [20,21].

2.3. ECG signal processing

For the Bordeaux dataset, we applied a Savitzky–Golay filter for baseline wander removal and a 3rd order Butterworth low-pass filter to remove high-frequency noise above 40 Hz. However, for the Utah datasets, we applied only the Butterworth low pass filter to eliminate high-frequency noise above 40 Hz. In the Utah datasets, representative beats used in this analysis were isolated, baseline corrected, filtered, and fiducialized using PFEIFER open-source platform [22].

2.4. Removal or interpolation of ECG leads deemed to be of lowest amplitude

For each dataset, low amplitude ECG leads were determined by sorting, in ascending order, all ECG leads (128 leads for the Bordeaux data and 192 leads for the Utah data) based on the peak-to-peak amplitude of the signal within the QRS complex ($A_{p\text{-}p}$). Fig. 1 (generated using Map3d [23]) shows the distribution of $A_{p\text{-}p}$ over the torso for each of the datasets (Utah and Bordeaux datasets).

Following that, we selected the *M* leads with the lowest $A_{p\text{-}p}$ and either removed them or replaced them with interpolated signals computed using one of several methods. The number of leads (M) was selected as follows: 1, 6, 11, 16, and 21. The methods used to replace the selected *M* leads with the lowest $A_{p\text{-}p}$ were as follows: 1. Removal, 2. Laplacian interpolation [7,10,12]. 3. Hybrid interpolation [11], 4. Inverse-Forward interpolation (IF) [10].

The Laplacian interpolation method is based on the physical properties that govern the behaviour of electrostatic potential in the volume conductor. Since the torso surface contains neither sources nor sinks, the Laplacian of the potential over the entire torso surface is zero. So, the unknown potentials are computed in a way that guarantees that the spatial second derivative of the potentials is smooth over the surface of the volume conductor [10]. Laplacian-based interpolation has been used previously to transform BSPMs recorded using one lead system to another lead system in order to pool or standardize body surface potential data from different research centres [13,14].

The hybrid interpolation method combines Laplacian interpolation and principal component analysis (PCA) interpolation [11]. In PCA interpolation, we suppose that we have at least one ECG beat over the entire torso surface. We used the PCA technique on the first beat to find new uncorrelated variables called the principal components (PCs) arranged in order of decreasing variance. We then predicted the values of potentials for the remaining beats using the first *n* principal components that account for most of the variability in the first beat. In the hybrid method, the number of principal components is selected to result in an

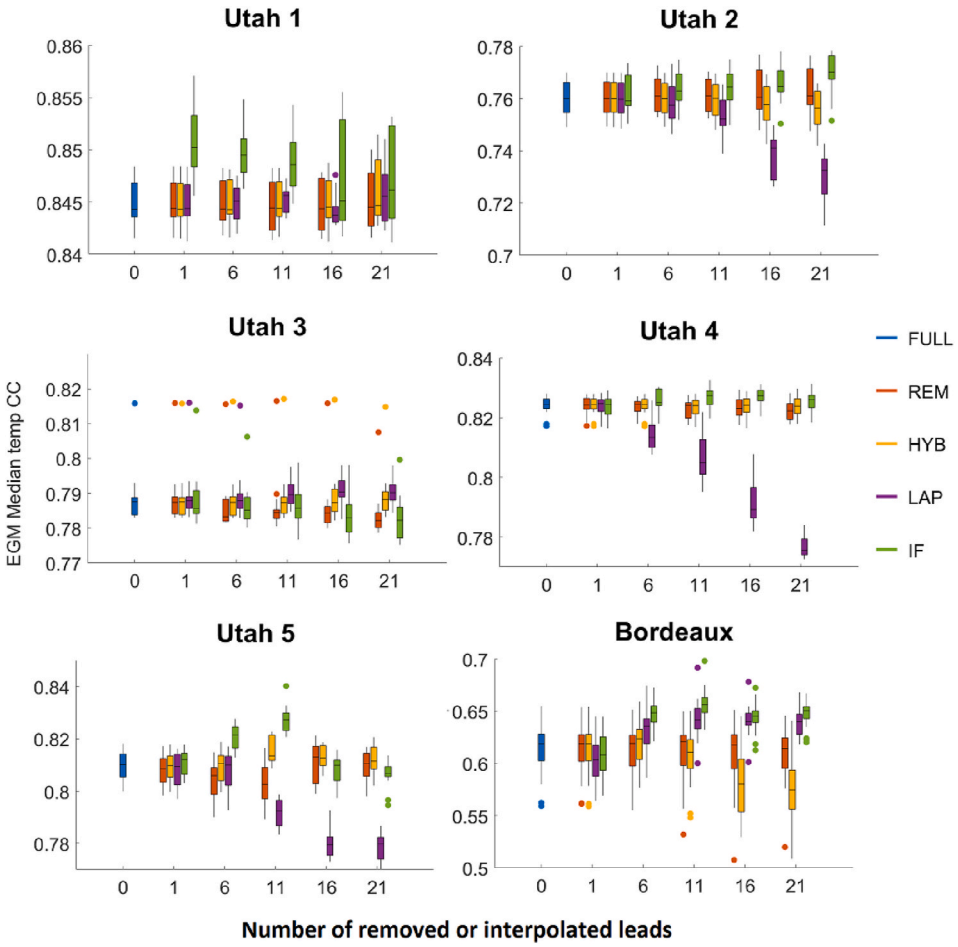

Fig. 5. The median of CC_{EGM} of EGMs for each of the six datasets. Each subplot shows the median of CC_{EGM} measured for FULL, REM, HYB, LAP, and IF methods as the number of removed or interpolated leads were increased. The median of CC_{EGM} values are expressed as median [lower quartile, upper quartile].

interpolated signal that is a trade-off between Laplacian interpolation and PCA interpolation [11].

The inverse-forward interpolation (IF) is a method described in Ref. [10]. Briefly, it uses the method of fundamental solutions to solve the inverse problem to calculate the potentials at a surface between the torso and the heart. The interpolated potentials are then computed by forward transforming the inner surface potentials to the outer surface.

Afterward, the recorded and the interpolated signals were segmented manually in the Bordeaux dataset and using PFEIFER software for Utah datasets. This resulted in 31, 12, 13, 14, 13, 12 beats for the Bordeaux, Utah 1, Utah 2, Utah 3, Utah 4, and Utah 5 datasets respectively.

2.5. Inverse reconstruction of cardiac electrical activity

Given the processed torso electrical potentials and the heart-torso geometries, we estimated the epicardial electrical potentials. We used the boundary element method [24] to compute the transfer coefficients (forward matrix) that relate the body surface potential distributions to the epicardial potential distributions based on the measurement of the heart-torso geometries [25].

$$V_{torso} = A\,V_{epi} + e$$

V_{torso}: is a vector of recorded torso potentials.
V_{epi} : is a vector of unknown epicardial potentials.
A : is the forward matrix.
e : is a vector of measurement noise.

Computing epicardial potentials from the potential measurements on the torso is the goal. This can be achieved by solving the inverse problem. However, the inverse problem is ill-posed which means that any small noise in the measurement can potentially be amplified in the solution. This can be overcome by regularization. We used zero-order Tikhonov regularization to regularize the solution [26]:

$$\min_{V_{epi}} \left[\|A V_{epi} - V_{torso}\|^2 + \lambda \|V_{epi}\|^2 \right], \tag{1}$$

where λ is the regularization parameter calculated using the L-curve which is a log-log plot of the regularized solution norm versus the corresponding residual norm. The inverse problem was solved using a single lambda value selected by finding the median of all lambda values computed at each time instant using the L-curve.

2.6. Methods of comparison

The performance of each method (Laplacian interpolation, Hybrid interpolation, Inverse forward interpolation) was assessed by comparing the interpolated ECGs with the recorded ECGs using two independent and widely used metrics; Pearson's correlation coefficient (CC) and normalized root mean square error (NRMSE) defined as shown in equations (2) and (3). Pearson's correlation coefficient (CC) was also used to compare the reconstructed electrograms (EGMs) after removing or interpolating low amplitude leads with the recorded EGMs.

$$CC = \frac{\sum_{i=1}^{n} \left(V_i^m - \overline{V^m}\right)\left(V_i^c - \overline{V^c}\right)}{\sqrt{\sum_{i=1}^{n} \left(V_i^m - \overline{V^m}\right)^2 \sum_{i=1}^{n} \left(V_i^c - \overline{V^c}\right)^2}} \tag{2}$$

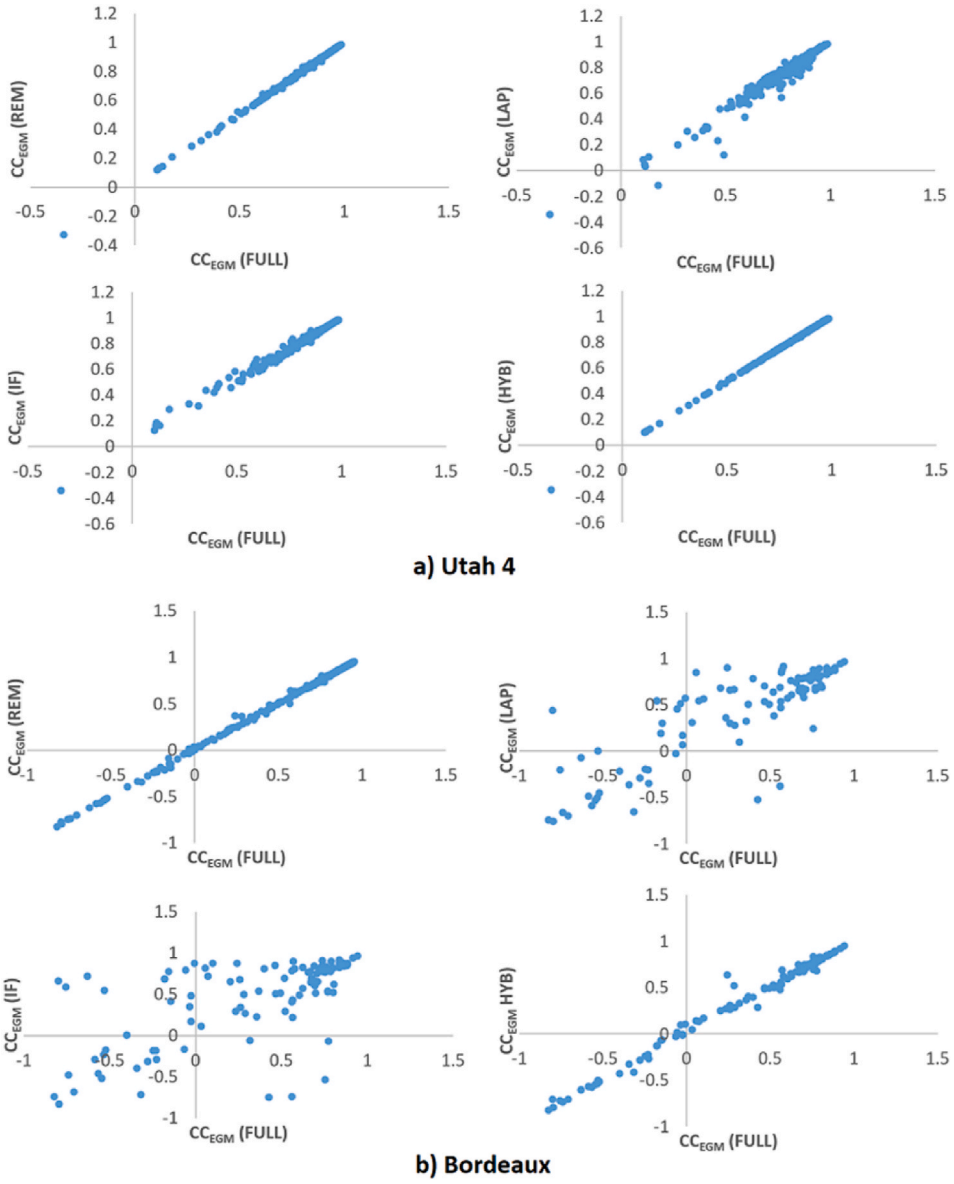

Fig. 6. Scatter plots for all datasets that display at one axis the CC_{EGM} (FULL) and at the other axis the CC_{EGM} (REM, LAP, HYB, or IF). The points above the identity line represent an improvement in the CC_{EGM}, whereas the points below the identity line represent a worsening in the CC_{EGM}.

$$NRMSE = \frac{\sqrt{\frac{\sum_{i=1}^{n}\left(V_i^m - V_i^c\right)^2}{n}}}{(\max V^m - min V^m)} \quad (3)$$

where:

n represents the number of temporal samples in the EGM or the ECG.

V_i^m denotes the measured potentials of the ith sample.

$\overline{V^m}$ denotes the average measured potential over all samples.

V_i^c indicates the calculated potentials of the ith sample.

$\overline{V^c}$ indicates the average calculated potential over all samples.

Ground truth activation times (AT_T) were computed as the moment of the steepest voltage downslope. However, the spatiotemporal approach that realizes that the activation times are not only dependent on the temporal signals but also on the spatial gradient of potentials between neighbouring nodes was used to compute the activation times from the reconstructed EGMs (AT_R) [27,28]. Following that, we compared AT_T and AT_R using Pearson's correlation coefficient.

For each beat in each dataset, five metrics were calculated at each electrode: CC_{ECG}: Pearson's correlation coefficient between the interpolated and recorded ECGs, $NRMSE_{ECG}$: normalized root mean square error between the interpolated and recorded ECGs, CC_{EGM}: Pearson's correlation coefficient between the reconstructed and recorded EGMs, CC_{AT}: Pearson's correlation coefficient between the reconstructed and Ground truth ATs, and localization error (LE). For each of the previously defined metrics, the median value across all electrodes was calculated, except CC_{AT} and LE which are already a single value for each beat.

2.7. Statistical analysis

The values of median CC_{ECG}, median $NRMSE_{ECG}$, median CC_{EGM}, CC_{AT} and LE across all beats are expressed as median [lower quartile, upper quartile]. The Wilcoxon signed-rank tests were performed for these metrics with $p < 0.05$ defined as significant.

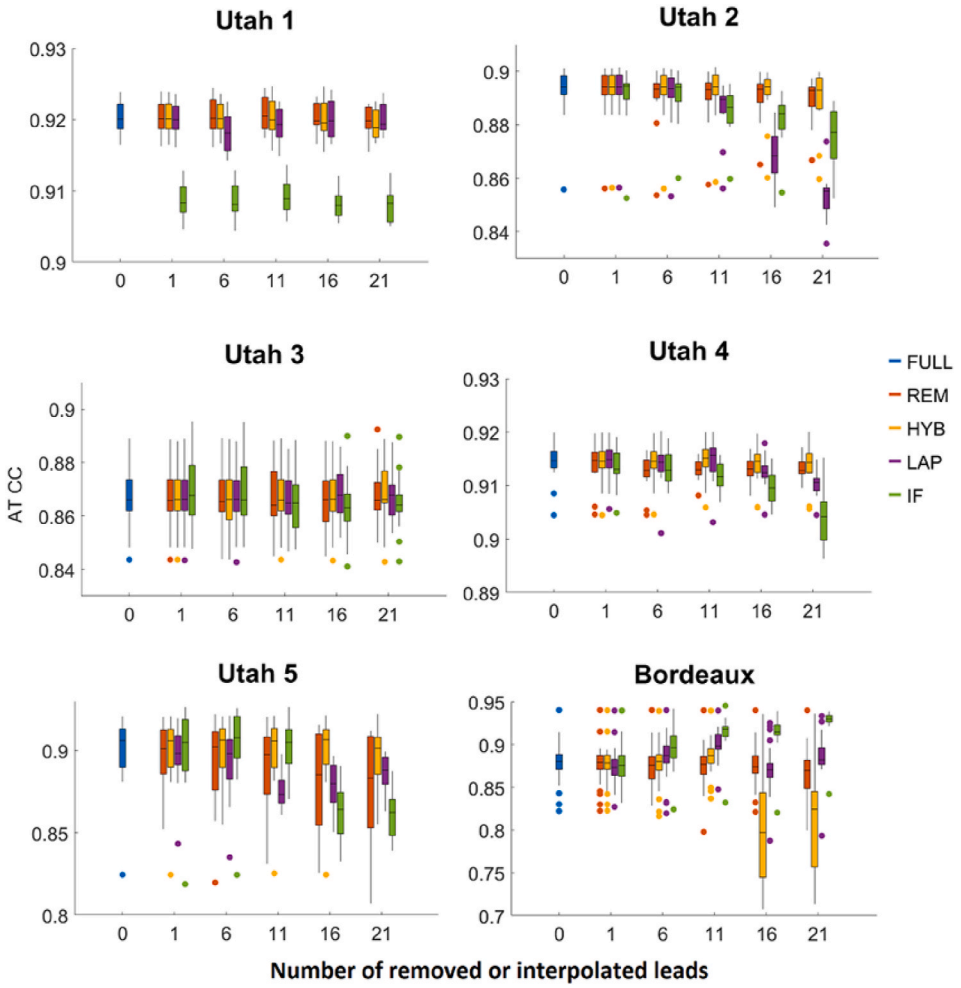

Fig. 7. The CC_{AT} for each of the six datasets. Each subplot shows the median of CC_{AT} measured for FULL, REM, HYB, LAP, and IF methods as the number of removed or interpolated leads were increased. The CC_{AT} values are expressed as median [lower quartile, upper quartile].

3. Results

3.1. ECG comparisons

Fig. 3 shows the median of $NRMSE_{ECG}$ as calculated between the recorded and interpolated ECGs. The hybrid method resulted in the lowest values for the median of $NRMSE_{ECG}$ ($p < 0.05$). On the other hand, the Laplacian interpolation largely exhibited the highest error in terms of the median of $NRMSE_{ECG}$. This was with the exception of when the Bordeaux dataset was studied.

The medians of CC_{ECG} between the recorded and interpolated ECGs are shown in Fig. 4. All interpolation methods resulted in highly correlated ECGs in Utah 1 and 3. The ECG signals interpolated using the hybrid method were the most correlated with the recorded ECGs except in the Bordeaux dataset when over 16 leads were interpolated. CC_{ECG} values were very low for the Laplacian interpolation method in Utah 4 and 5. These values were also very low for the IF interpolation method in Utah 2 and Bordeaux datasets.

3.2. EGM comparisons

Fig. 5 presents the median of CC_{EGM} for each of the six datasets. As can be seen, there was no significant change in the median of CC_{EGM} when removing the low amplitude leads of up to 11 leads in all datasets as compared to when using the full set of leads. Furthermore, Laplacian and hybrid interpolating low amplitude leads did not improve the inverse solution. Instead, they worsened the reconstructed EGMs in some datasets. For example, In Utah 4, when Laplacian interpolation was used over 21 leads, the median CC was reduced from 0.825 [0.823, 0.826] to 0.776 [0.774, 0.779] ($p < 0.05$) compared to using the full set for reconstructing (Fig. 5). Hybrid interpolation also worsened the inverse solution for the Bordeaux dataset where median CC_{EGM} decreased from 0.619 [0.603, 0.628] to 0.575 [0.556, 0.594] ($p < 0.05$) when removing the 21 leads as compared to using the full set of leads. Inverse-forward interpolation improved the inverse reconstruction in the Bordeaux dataset, where the median CC_{EGM} started at 0.619 [0.603, 0.628] without interpolation, peaked at 0.656 [0.649, 0.663] when interpolating 11 electrodes, and then remaining at 0.65[0.643, 0.654] when interpolating 21 electrodes ($p < 0.05$). In Utah 5, the median CC_{EGM} increased from 0.81 [0.805, 0.814] to 0.827 [0.823, 0.83] and then decreased to 0.807 [0.806, 0.809] when IF interpolating the 0, 11, or 21 leads with the lowest $A_{p\text{-}p}$, respectively ($p < 0.05$). The change in the median CC_{EGM} for Utah 1 to Utah 4 was slight and insignificant when using the IF interpolation method.

Fig. 6 shows scatter plots that display the values of two variables: the first one is the correlation coefficient between the recorded EGMs and the reconstructed EGMs using the full set of leads (CC_{EGM} (FULL)), and the second variable is the correlation coefficient between the recorded EGMs and the reconstructed EGMs when 11 leads with the lowest $A_{p\text{-}p}$ were removed or interpolated (CC_{EGM} (Inter or REM)). These plots help in identifying the sock electrodes where the reconstructed EGMs were improved or worsened. The points above the identity line correspond to

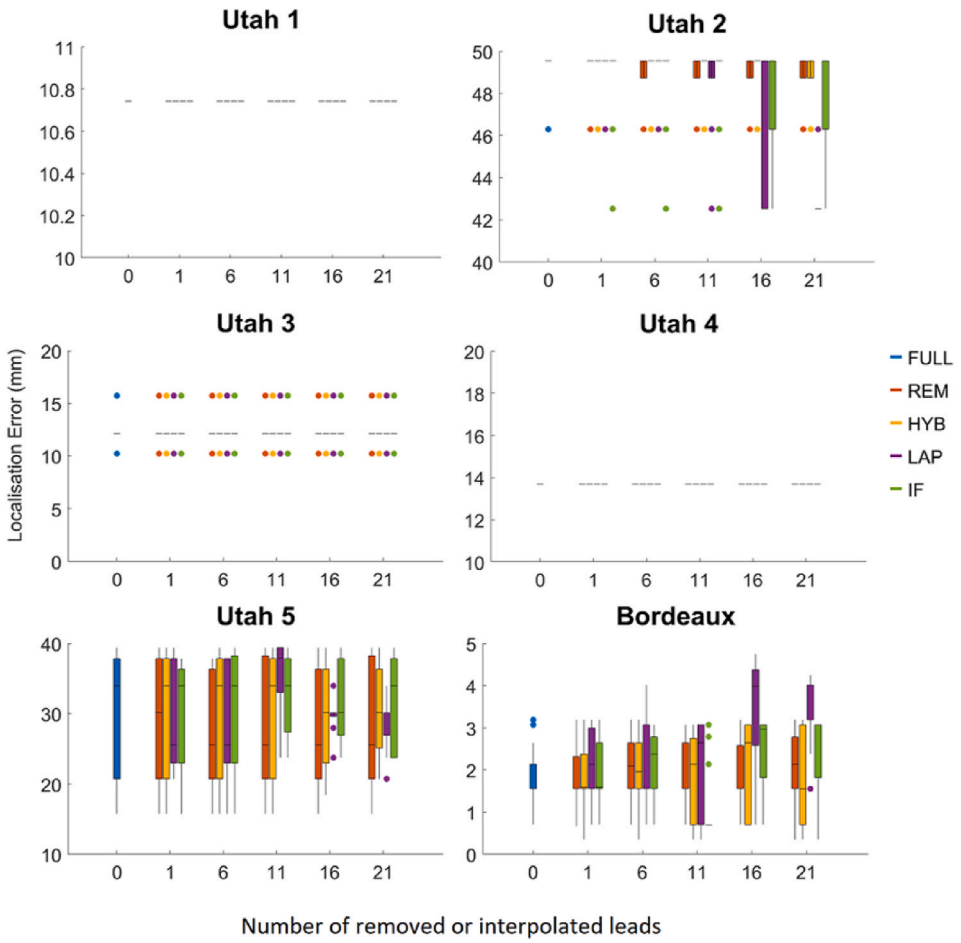

Fig. 8. The localization error for each of the six datasets. Each subplot shows the median of localization error (LE) measured for FULL, REM, HYB, LAP, and IF methods as the number of removed or interpolated leads were increased. The LE values are expressed as median [lower quartile, upper quartile].

improvements in the reconstructed EGMs, whereas those below the identity line correspond to worsening in the reconstructed EGMs. Fig. 6a (Utah 4) shows an example where there was a slight change in the CC values when using FULL, REM, HYB, or IF methods. LAP method resulted in a worsening in the inverse reconstruction as shown in Fig. 6a. Whereas, the change in the inverse reconstruction is higher in the Bordeaux dataset (Fig. 6b). It is apparent that IF interpolation achieved the best results in terms of improving the CC_{EGM} values. These results are in agreement with the results showed in Fig. 5.

3.3. AT comparisons

Fig. 7 presents the change in the CC_{AT} as we remove or interpolate more leads in all datasets. There was no significant change in the median of CC_{AT} when removing the low amplitude leads of up to 11 leads in all datasets as compared to when using the full set of leads. There was a significant decrease in the CC_{AT} when Laplacian interpolation was used over more electrodes in Utah 2, with CC_{AT} decreased from 0.85 ± 0.023 to 0.81 ± 0.02 ($p < 0.05$) after 21 leads were interpolated. The same trend was noticed when we used the hybrid interpolation in the Bordeaux dataset with numbers decreased from 0.87 ± 0.028 to 0.80 ± 0.06 for 0 and 21 leads respectively. However, there was a significant increase when the IF interpolation was used for the Bordeaux dataset, increasing to 0.93 ± 0.02 for 21 leads ($p < 0.05$).

3.4. Localization error

Fig. 8 shows the localization error which is the distance between the true pacing site and the computed pacing site using the activation times derived from the reconstructed EGMs. In Utah 1 and Utah 4, the localization error was approximately fixed at 10.74 and 13.69 mm respectively. In Utah 3, apart from the few outliers shown in the figure, the localization error was approximately 12.13 mm. There was no significant difference in the localization error between different methods of interpolation in these datasets (Utah 1, Utah 2, and Utah 3). This is because the different methods of interpolation did not impact the reconstructed epicardial potentials especially at the region around the pacing site. We noticed that there is a variation in the localization error between the different methods of interpolation and between different beats in Utah 5 and Bordeaux datasets. This might be because the interpolated low amplitude leads are located above the pacing site in these two datasets as shown in Fig. 2. In the Bordeaux dataset, the IF interpolation of the 11 leads with the lowest $A_{p\text{-}p}$ reduced the median of the localization error significantly.

3.5. AT and CC maps

Fig. 9 presents the CC maps for all datasets when the full set of leads (FULL), the 11 electrodes with the lowest $A_{p\text{-}p}$ removed (REM), or interpolated using HYB, LAP, or IF interpolation methods were used for solving the inverse problem of electrocardiography. The results in these maps are in agreement with the results shown previously in Fig. 5. There was no significant change in the CC map between the different methods in Utah 1 to 3. In Utah 4 and 5, it can be noticed that the Laplacian method worsened the CC map in some regions of the heart. This worsening in the CC map is marked by the widening of the blue region. The IF

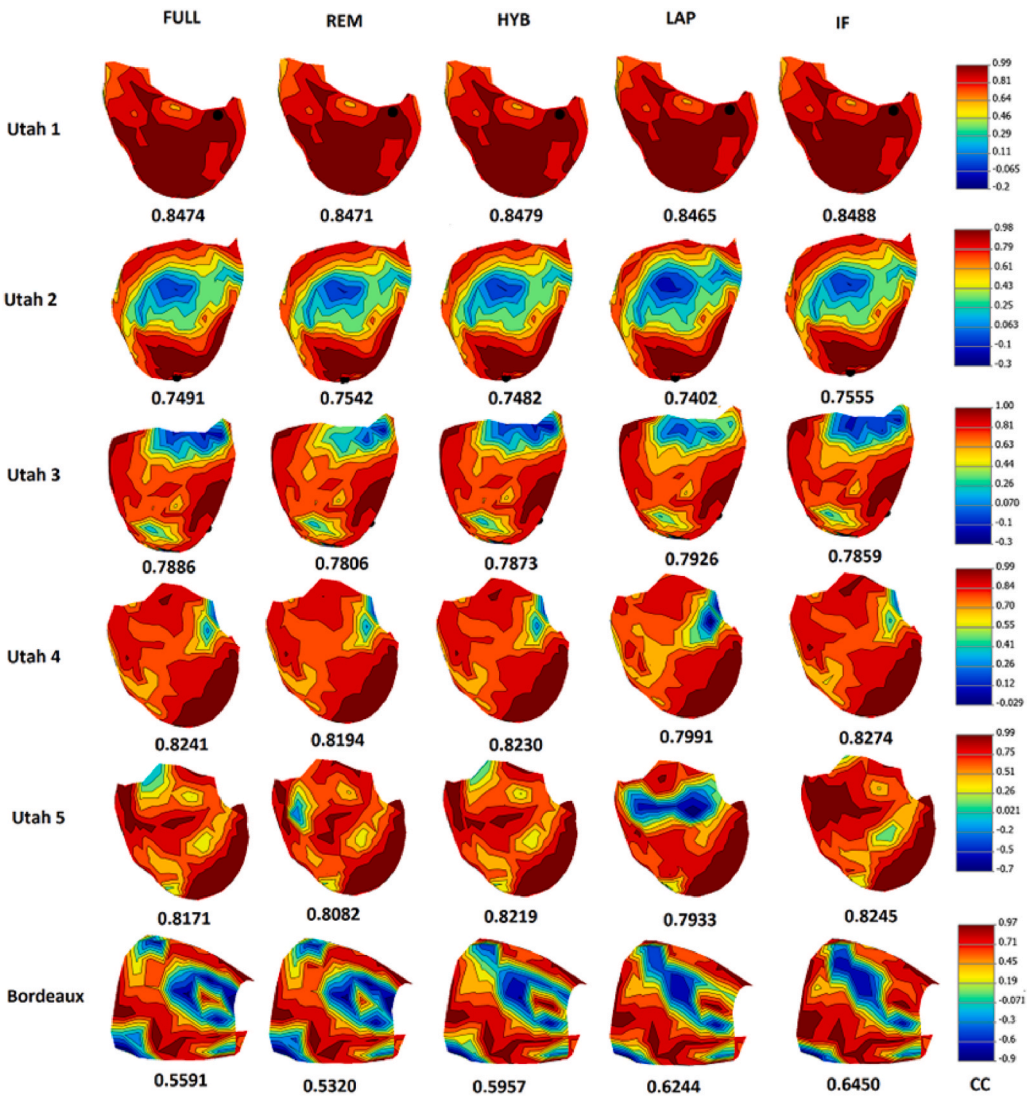

Fig. 9. Correlation coefficient maps (CC maps) for each of the six datasets when 11 leads with the lowest $A_{p\text{-}p}$ were removed or interpolated.

interpolation method improved the CC map in some regions on the heart in Utah 5 and Bordeaux datasets as presented in Fig. 9. This is also apparent from the change in the CC from 0.8171 to 0.5591 to 0.8245 and 0.645 in Utah 5 and Bordeaux datasets respectively. It is clear the widening in the red region in the CC map for Utah 5 and Bordeaux datasets which indicates the improvement in the inverse solution.

Fig. 10 shows how interpolating the 11 body surface leads in Utah 5 (Fig. 10A) using the inverse-forward interpolation improved the reconstructed EGMs at nodes 1, 2, and 3 and the surrounding region. At these nodes, the CC_{EGM} increased from 0.557, 0.169, 0.031 to 0.882, 0.840, 0.674. The CC_{EGM} maps between the ground truth EGMs and reconstructed EGMs are shown in Fig. 10B (EGMs were reconstructed using the full set of leads) and Fig. 10C (EGMs were reconstructed after IF interpolating the 11 leads with the lowest $A_{p\text{-}p}$). We can see from Fig. 10D how the reconstructed EGMs were improved to become closer to the recorded EGMs. The activation time maps derived from the recorded EGMs, reconstructed EGMs using the full set, and reconstructed EGMs after IF interpolation of the 11 leads with the lowest $A_{p\text{-}p}$ are shown in Fig. 10E. The correlation between the ground truth AT map and the reconstructed AT map is higher for the IF interpolation (CC_{AT} = 0.91) than the full set (CC_{AT} = 0.89).

The enhancement in the reconstructed EGMs is more apparent in Bordeaux dataset than in the others. Fig. 11 shows that the enhancements are mainly in two regions (see the CC maps, EGMs plots, and AT maps). There was a substantial increase in the CC of the reconstructed EGMs with the recorded EGMs at nodes 1 to 6. The figures increased from −0.006, 0.106, −0.058, −0.757, −0.530, −0.629 to become 0.877, 0.877, 0.797, 0.591, 0.548, and 0.719. The activation time maps derived from the recorded EGMs, reconstructed EGMs using the full-set, and reconstructed EGMs after IF interpolation of the 11 leads with the lowest $A_{p\text{-}p}$ are shown in Fig. 8E. The AT map (IF interpolation, CC = 0.902) is more correlated with the AT map (Ground truth) than AT map (Full set, CC = 0.845).

It has been noticed that the number of the low amplitude leads that should be interpolated to improve or at least does not harm the inverse reconstruction should not exceed 11 electrodes. We found that this number of leads can be determined by selecting a threshold of 0.02. This threshold was computed by finding the percentage of the sum of peak-to-peak amplitudes of low amplitude leads to the sum of peak-to-peak amplitudes of all leads.

In order to determine the reason behind the improvements seen in reconstructions with interpolation, we analysed the lambda values used for regularization as computed using the L-curve method for each beat and compared these to an optimum lambda value. The optimum lambda was defined as the lambda value that gives the best solution in terms of the highest CC_{EGM}. Although the optimum lambda value shown in Table 1 is one value for each beat, there is a range of values for lambda where the highest CC_{EGM} occurs. For simplicity, the reported lambda

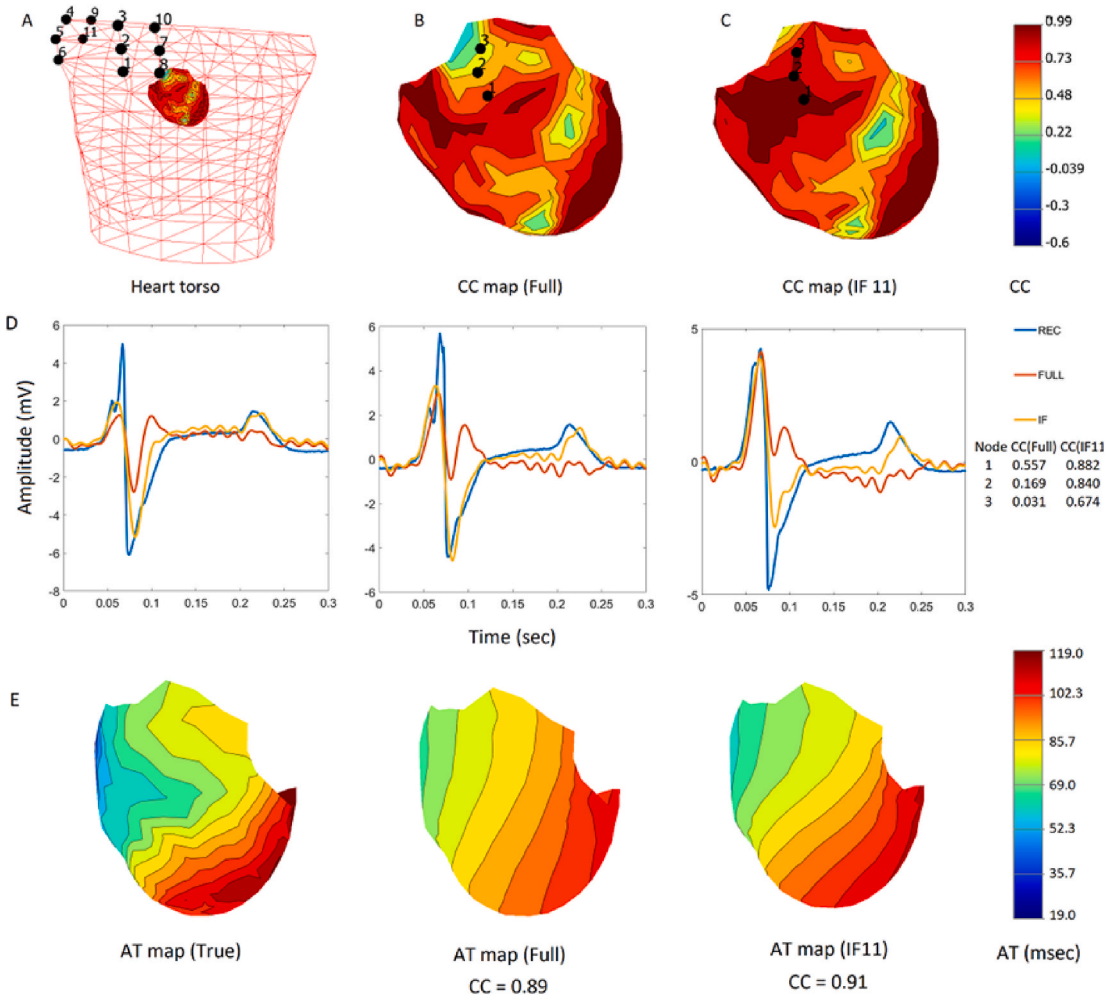

Fig. 10. A) The black dots represent the 11 leads with the lowest $A_{p\text{-}p}$ that were interpolated or removed. B) CC_{EGM} map between the recorded EGMs and reconstructed EGMs using the full set of leads. C) CC_{EGM} map between the recorded EGMs and reconstructed EGMs after IF interpolating the 11 leads with the lowest $A_{p\text{-}p}$. D) EGMs recorded or reconstructed at the nodes 1,2, and 3 shown in B and C. E) Activation time map derived from the recorded EGMs (Left) vs derived from the reconstructed EGMs using the full set (Middle) and that derived from the reconstructed EGMs using IF interpolation the 11 leads with the lowest $A_{p\text{-}p}$ (Right).

value in the table is one value for each beat. In Table 1, the median CC_{EGM} was calculated for each beat and the median (min-max) across all beats is shown in Table 1 for reconstruction using the full data set, the IF interpolation of 11 electrodes with the L-curve method to define lambda, and the using the full data set but with the optimal lambda value. This explains that there is an improvement in the solution in Utah 5 and Bordeaux and no improvement in Utah 1 to 4 after IF interpolating the lowest amplitude signals. IF interpolating helps in finding a better lambda that could improve the solution. Fig. 12 shows some examples of the L-curve and how the selected lambda value becomes closer to the optimum lambda when the IF interpolation was performed for the 11 leads with the lowest $A_{p\text{-}p}$ amplitude.

4. Discussion

This study investigated the effect of removal or interpolating low amplitude signals on the inverse reconstruction of cardiac electrical activity. Body surface signals were ranked based on their peak-to-peak amplitude over the QRS complex. Measured low amplitude signals were removed or replaced with interpolated signals before computing the inverse solution. IF interpolation, Laplacian interpolation, and hybrid interpolation were used and compared.

Although the hybrid method was successful in interpolating the low amplitude leads with a higher correlation coefficient and lower NRMSE values as compared to the IF interpolation method, it did not result in a better inverse reconstruction of the cardiac electrical activity. This is because other parameters such as the regularization parameter can play an important role in getting a better inverse solution.

The Laplacian interpolation that has been used as a method to transform BSPMs recorded using one lead system to another lead system in order to pool or standardize body surface potential data from different research centres [13,14] did not perform very well in interpolating low amplitude leads. This is apparent from the worsening in the reconstructed EGMs and activation times derived from them when this method was used.

The Inverse forward interpolation (IF) performed better than other interpolation methods. This is not surprising, given the effectiveness of this method over other interpolation methods has previously been reported [6,10]. This is because this method considers the physics of the problem that describe the electromagnetic field in the torso volume conductor. What is surprising is that when we interpolate some electrodes, although some information was lost, a better or at least the same reconstruction was achieved. That is IF interpolation of the low amplitude signals improved the inverse solution in Bordeaux and Utah 5. However, no substantial change was noticed in the other datasets (Utah 1, Utah 2, Utah3, and Utah 4) when using the IF interpolation method.

The explanation for this improvement is that the interpolation contributed to the regularization of the solution. An infinite number of

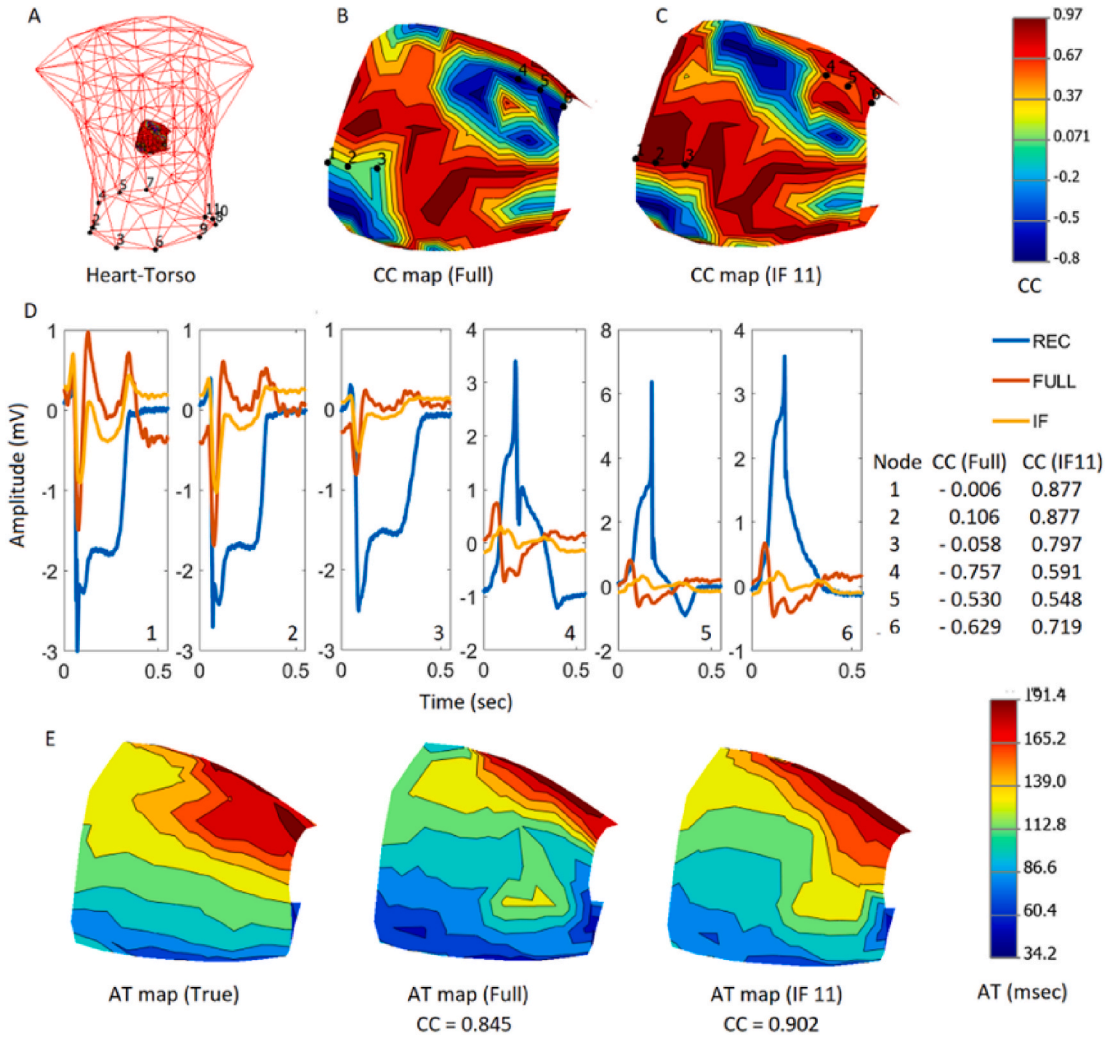

Fig. 11. A) The black dots represent the 11 leads with the lowest $A_{p\text{-}p}$ that were interpolated or removed. B) CC_{EGM} map between the recorded EGMs and reconstructed EGMs using the full set of leads. C) CC_{EGM} map between the recorded EGMs and reconstructed EGMs after IF interpolating the 11 leads with the lowest $A_{p\text{-}p}$. D) EGMs recorded or reconstructed at the nodes 1,2, and 3 shown in B and C. E) Activation time map derived from the recorded EGMs (Left) vs derived from the reconstructed EGMs using the full set (Middle) and that derived from the reconstructed EGMs using IF interpolation the 11 leads with the lowest $A_{p\text{-}p}$ (Right).

Table 1
The median of CC_{EGM} between true and reconstructed EGMs using Lambda selected using the L-curve approach or using the best possible Lambda.

Dataset	median of CC_{EGM} Full set (λ: L-curve)	Lambda values (Full)	median of CC_{EGM} IF 11 (λ: L-curve)	Lambda values (IF 11)	median of CC_{EGM} Full set (Optimum λ)	Lambda values (Optimum)
Utah 1	0.845 (0.842–0.851)	0.0094 [0.0093, 0.0096]	0.849 (0.845–0.856)	0.0096 [0.0095–0.0098]	0.856 (0.849–0.859)	0.0114 [0.0134–0.0150]
Utah 2	0.76 (0.749–0.77)	0.0126 [0.0123–0.0134]	0.765 (0.75–0.775)	0.0130 [0.0128, 0.0137]	0.765 (0.754–0.777)	0.0137 [0.0126–0.0148]
Utah 3	0.788 (0.78–0.80)	0.0090 [0.0090–0.0093]	0.786 (0.777–0.8)	0.0096 [0.0094–0.0098]	0.792 (0.787–0.80)	0.0078 [0.0074–0.0082]
Utah 4	0.825 (0.817–0.828)	0.0138 [0.0135–0.0140]	0.827 (0.82–0.833)	0.137 [0.0135–0.0140]	0.826 (0.821–0.834)	0.0113 [0.0104–0.0131]
Utah 5	0.81 (0.80–0.818)	0.0022 [0.0021–0.0024]	0.827 (0.821–0.84)	0.0030 [0.0030–0.0032]	0.821 (0.812–0.828)	0.0088 [0.0072–0.0167]
Bordeaux	0.619 (0.559–0.655)	0.0017 [0.0014–0.0019]	0.656 (0.63–0.698)	0.0033 [0.0030–0.0036]	0.666 (0.64–0.683)	0.0049 [0.0035–0.0058]

solutions satisfy the equations of this problem, and the best solution is selected by regularization. For Bordeaux and Utah 5 datasets, interpolation improved the choice of the regularization parameter compared to the other Utah datasets where choosing other values for lambda did not improve the solution. This change in the regularization parameter was noticed as we interpolate (IF) more electrodes in Bordeaux and Utah 5. In other words, when interpolating these low amplitude signals using the IF method, although we might lose some information, we allow for choosing a better value for the regularization parameter that gives a better inverse reconstruction. The stability of lambda values in Utah 1 to Utah 4 datasets as we interpolate more electrodes using the IF method indicates that the regularization in these datasets is sufficient and no more regularization is needed.

5. Conclusion

Removal of low amplitude signals of up to 11 leads did not change the reconstructed EGMs or the activation maps derived from them. In addition, interpolating low amplitude signals using the Laplacian or the Hybrid method improved the inverse solution in some datasets but worsened it in other datasets. Furthermore, IF interpolating the lowest amplitude signals of up to 11 electrodes improved the reconstructed

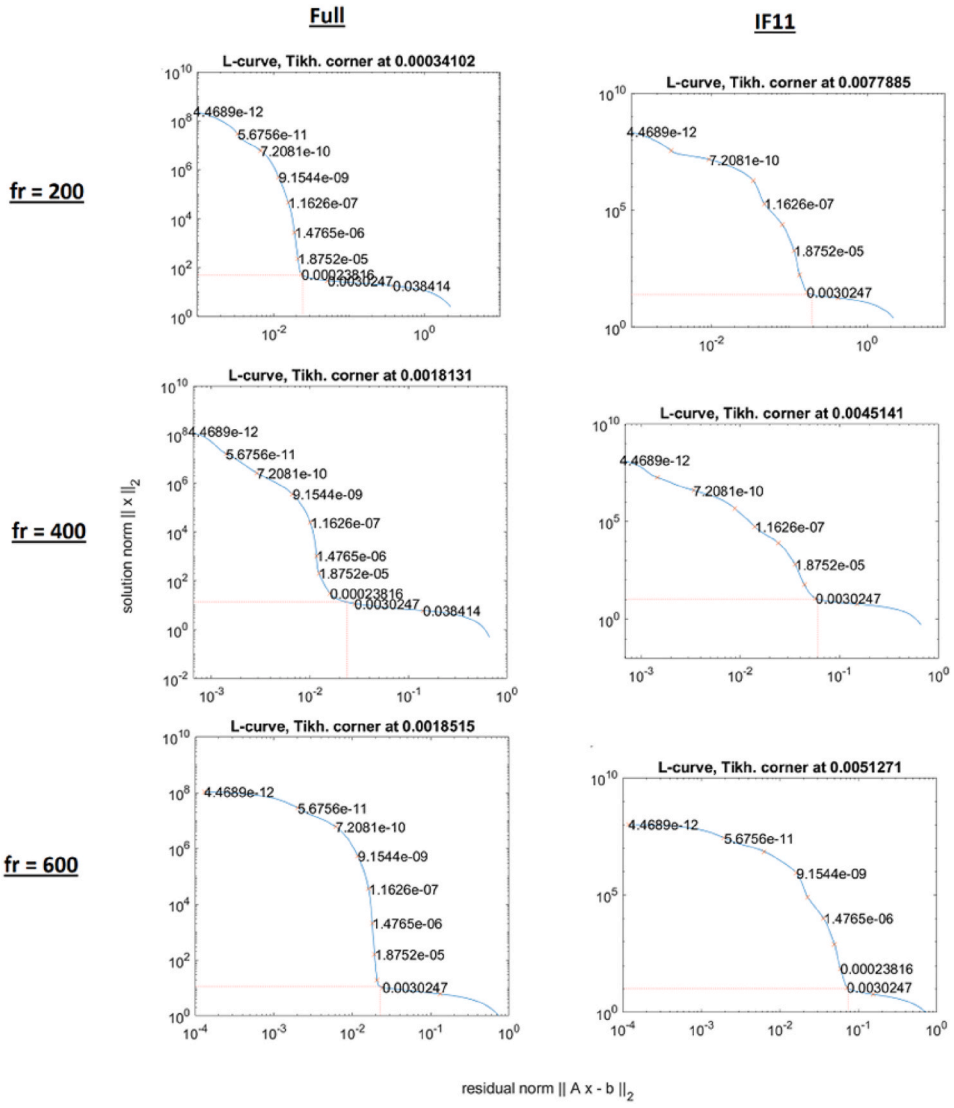

Fig. 12. a set of plots for the L-curve used for identifying the appropriate lambda for regularizing the inverse solution for the Bordeaux dataset. These plots show the change in the selected lambda when 11 leads with the lowest $A_{p\text{-}p}$ were interpolated using IF interpolation as compared to using the full set of leads.

EGMs and the AT maps in some datasets and at the same time did not significantly worsened the reconstructed EGMs AT maps in the rest of the datasets. More importantly, despite a potential loss of BSPM information when using IF interpolation on low amplitude signals, inverse solutions can be improved by altering the L-curve and allowing a more optimal regularization parameter to be selected. This improvement is not seen by simply removing low amplitude signals.

Declaration of competing interest

The authors declare that they have no known competing financial interests or personal relationships that could have appeared to influence the work reported in this paper.

Acknowledgments

This project is part of the Eastern Corridor Medical Engineering center (ECME). It is supported by the European Union's INTERREG VA Programme, managed by the Special EU Programmes Body (SEUPB). This project was also supported by the National Institute of General Medical Sciences of the National Institutes of Health under grant number P41 GM103545-18 and the Nora Eccles Treadwell Foundation at the Cardiovascular Research and Training Institute (CVRTI) funded the experiment data collection. This work was also supported by the French National Research Agency (ANR-10-IAHU04-LIRYC).

References

[1] Y. Wang, P.S. Cuculich, J. Zhang, K.A. Desouza, R. Vijayakumar, J. Chen, M. N. Faddis, B.D. Lindsay, T.W. Smith, Y. Rudy, Noninvasive electroanatomic mapping of human ventricular arrhythmias with electrocardiographic imaging (ECGI), Sci. Transl. Med. 3 (2011) 98ra84, https://doi.org/10.1126/scitranslmed.3002152.

[2] M. Cluitmans, D.H. Brooks, R. MacLeod, O. Dössel, M.S. Guillem, P.M. Van Dam, J. Svehlikova, B. He, J. Sapp, L. Wang, L. Bear, Validation and Opportunities of Electrocardiographic Imaging: from Technical Achievements to Clinical Applications, 2018.

[3] R.S. MacLeod, D.H. Brooks, Recent Progress in Inverse Problems in Electrocardiology, 1998.

[4] L.R. Bear, Y.S. Doz, J. Svehlikova, J. Coll-Font, W. Good, E. Van Dam, R. Macleod, E. Abell, R. Walton, R. Coronel, M. Haissaguerre, R. Dubois, Effects of ECG signal processing on the inverse problem of electrocardiography, in: Computing in Cardiology, IEEE Computer Society, 2018.

[5] L.R. Bear, Y. Serinagaoglu, W.W. Good, J. Svehlikova, J. Coll-Font, E. van Dam, R. MacLeod, The impact of torso signal processing on noninvasive electrocardiographic imaging reconstructions, IEEE Trans. Biomed. Eng. (2020), https://doi.org/10.1109/tbme.2020.3003465, 1–1.

[6] Y.S. Dogrusoz, L.R. Bear, J. Bergquist, R. Dubois, W. Good, R.S. Macleod, A. Rababah, J. Stoks, Effects of interpolation on the inverse problem of electrocardiography, in: Computing in Cardiology, 2019.
[7] A.S. Rababah, D.D. Finlay, D. Guldenring, R. Bond, J. Mclaughlin, An Adaptive Laplacian Based Interpolation Algorithm for Noise Reduction in Body Surface Potential Maps, 2018.
[8] E. Deutsch, J. Svehlikova, M. Tysler, P. Osmancik, J. Zdarska, P. Kneppo, Effect of elimination of noisy ECG leads on the noninvasive localization of the focus of premature ventricular complexes, in: IFMBE Proceedings, Springer Verlag, 2019, pp. 75–79.
[9] A. Rababah, D. Finlay, L. Bear, R. Bond, K. Rjoob, J. Mclaughlin, Interpolating low amplitude ECG signals combined with filtering according to international standards improves inverse reconstruction of cardiac electrical activity, in: Lecture Notes in Computer Science (Including Subseries Lecture Notes in Artificial Intelligence and Lecture Notes in Bioinformatics), Springer Verlag, 2019, pp. 112–120.
[10] J.E. Burnes, D.C. Kaelber, B. Taccardi, R.L. Lux, P.R. Ershler, Y. Rudy, A field-compatible method for interpolating biopotentials, Ann. Biomed. Eng. 26 (1998) 37–47, https://doi.org/10.1114/1.49.
[11] A.S. Rababah Msc, R.R. Bond, K.R. Msc, D. Guldenring, J. McLaughlin, D.D. Finlay, Novel hybrid method for interpolating missing information in body surface potential maps, J. Electrocardiol. 57 (2019) S51–S55, https://doi.org/10.1016/j.jelectrocard.2019.09.003.
[12] T.F. Oostendorp, A. van Oosterom, G. Huiskamp, Interpolation on a triangulated 3D surface, J. Comput. Phys. 80 (1989) 331–343, https://doi.org/10.1016/0021-9991(89)90103-4.
[13] R. Hoekema, G.J.H. Uijen, A. Van Oosterom, On selecting a body surface mapping procedure. https://pubmed.ncbi.nlm.nih.gov/10338028/.
[14] R. Hoekema, G.J.H. Uijen, A. van Oosterom, Lead system transformation for pooling of body surface maps: an evaluation, in: Annual International Conference of the IEEE Engineering in Medicine and Biology - Proceedings, IEEE, 1996, pp. 1413–1414.
[15] A. Ghodrati, D.H. Brooks, R.S. MacLeod, Methods of solving reduced lead systems for inverse electrocardiography, IEEE Trans. Biomed. Eng. 54 (2007) 339–343, https://doi.org/10.1109/TBME.2006.886865.
[16] A.K. Evans, R.L. Lux, M.J. Burgess, R.F. Wyatt, J.A. Abildskov, Redundancy reduction for improved display and analysis of body surface potential maps. II. Temporal compression, Circ. Res. 49 (1981) 197–203, https://doi.org/10.1161/01.RES.49.1.197.
[17] R.L. Lux, A.K. Evans, M.J. Burgess, R.F. Wyatt, J.A. Abildskov, Redundancy reduction for improved display and analysis of body surface potential maps. I. Spatial compression, Circ. Res. 49 (1981) 186–196, https://doi.org/10.1161/01.RES.49.1.186.
[18] R.C. Barr, M.S. Spach, G.S. Herman-Giddens, Selection of the number and positions of measuring locations for electrocardiography, IEEE Trans. Biomed. Eng. BME- 18 (1971) 125–138, https://doi.org/10.1109/TBME.1971.4502813.
[19] L.R. Bear, P.R. Huntjens, R.D. Walton, O. Bernus, R. Coronel, R. Dubois, Cardiac electrical dyssynchrony is accurately detected by noninvasive electrocardiographic imaging, Heart Rhythm 15 (2018) 1058–1069, https://doi.org/10.1016/j.hrthm.2018.02.024.
[20] S. Shome, R. Macleod, Simultaneous high-resolution electrical imaging of endocardial, epicardial and torso-tank surfaces under varying cardiac metabolic load and coronary flow, in: Lecture Notes in Computer Science (Including Subseries Lecture Notes in Artificial Intelligence and Lecture Notes in Bioinformatics), Springer Verlag, 2007, pp. 320–329.
[21] B. Zenger, W.W. Good, J.A. Bergquist, B.M. Burton, J.D. Tate, L. Berkenbile, V. Sharma, R.S. MacLeod, Novel experimental model for studying the spatiotemporal electrical signature of acute myocardial ischemia: a translational platform, Physiol. Meas. 41 (2020), https://doi.org/10.1088/1361-6579/ab64b9.
[22] A. Rodenhauser, W. Good, B. Zenger, J. Tate, K. Aras, B. Burton, S. MacLeod, R.: PFEIFER: preprocessing framework for electrograms intermittently fiducialized from experimental recordings, J. Open Source Softw. 3 (2018) 472, https://doi.org/10.21105/joss.00472.
[23] MacLeod, R.S., Johnson, C.R.: Map3d: Interactive Scientific Visualization for Bioengineering Data..
[24] R.C. Barr, M. Ramsey, M.S. Spach, Relating epicardial to body surface potential distributions by means of transfer coefficients based on geometry measurements, IEEE Trans. Biomed. Eng. BME- 24 (1977) 1–11, https://doi.org/10.1109/TBME.1977.326201.
[25] B.M. Burton, J.D. Tate, B. Erem, D.J. Swenson, D.F. Wang, M. Steffen, D.H. Brooks, P.M. Van Dam, R.S. MacLeod, A toolkit for forward/inverse problems in electrocardiography within the SCIRun problem solving environment, in: Proceedings of the Annual International Conference of the IEEE Engineering in Medicine and Biology Society, EMBS, 2011, pp. 267–270.
[26] A.N. Tikhonov, A.V. Goncharsky, V.V. Stepanov, A.G. Yagola, Numerical Methods for the Solution of Ill-Posed Problems, Springer Netherlands, 1995.
[27] B. Erem, D.H. Brooks, P.M. Van Dam, J.G. Stinstra, R.S. MacLeod, Spatiotemporal estimation of activation times of fractionated ECGs on complex heart surfaces, in: Proceedings of the Annual International Conference of the IEEE Engineering in Medicine and Biology Society, 2011, pp. 5884–5887.
[28] M. Cluitmans, J. Coll-Font, B. Erem, D. Brooks, Spatiotemporal activation time estimation improves noninvasive localization of cardiac electrical activity, in: Computing in Cardiology, IEEE Conference Publication, 2016, pp. 1185–1188.